JOURNAL OF GEOPHYSICAL RESEARCH, VOL. 111, D12211, doi:10.1029/2004JD005707, 2006

Path length distributions for solar photons under cloudy skies: Comparison of measured first and second moments with predictions from classical and anomalous diffusion theories

T. Scholl,[1] K. Pfeilsticker,[1] A. B. Davis,[2] H. Klein Baltink,[3] S. Crewell,[4,5] U. Löhnert,[4,5] C. Simmer,[4] J. Meywerk,[6] and M. Quante[6]

Received 16 December 2004; revised 5 October 2005; accepted 14 March 2006; published 27 June 2006.

[1] Using high-resolution oxygen A band spectrometry ($\lambda/\Delta\lambda = 60000$) in the 767.7–770.7 nm wavelength range, we investigate the first and second moments of the distributions of path lengths of photons in transmitted skylight for different cloud conditions. Our observations are supported by measurements of column liquid water path by multichannel microwave radiometry, cloud structure by millimeter cloud radar observations, and cloud base by a laser ceilometer. For the investigated multilayer cloud covers (decks of stratus, cumulus, altostratus, and cirrus), our measurements indicate that the photon path statistics are mostly governed by anomalous diffusion, whereby classical diffusion occurs in the limiting case of a single compact (plane parallel) cloud layer. The ratio for the inferred second and first moments of the path lengths confirms the relation recently derived by Davis and Marshak (2002) for photon diffusion in single optically thick cloud layers and extends it to more complex cloud geometry.

Citation: Scholl, T., K. Pfeilsticker, A. B. Davis, H. Klein Baltink, S. Crewell, U. Löhnert, C. Simmer, J. Meywerk, and M. Quante (2006), Path length distributions for solar photons under cloudy skies: Comparison of measured first and second moments with predictions from classical and anomalous diffusion theories, *J. Geophys. Res.*, *111*, D12211, doi:10.1029/2004JD005707.

1. Introduction

[2] Atmospheric absorption in the oxygen A band (≈770 nm) has been studied extensively in remote sensing for retrieval of surface pressure and cloud top heights from satellite measurements [*Grechko et al.*, 1973; *Fischer and Grassl*, 1999a, 1991b; *O'Brien and Mitchell*, 1992]. More recently, efforts have been made to use ground-based A band measurements at moderate to high spectral resolution to infer the distribution of photon path lengths, and to relate these to column cloud properties [*Harrison and Min*, 1997; *Pfeilsticker et al.*, 1998a; *Veitel et al.*, 1998; *Min and Harrison*, 1999; *Portmann et al.*, 2001; *Min et al.*, 2001; *Funk and Pfeilsticker*, 2003; *Min and Clothiaux*, 2003; *Min et al.*, 2004]. Simultaneously, there is a renewed interest in using the A band to assess the internal variability of clouds from spaceborne instruments [*Stephens and Heidinger*, 2000; *Heidinger and Stephens*, 2000, 2002; *Stephens et al.*, 2005].

[3] Using oxygen A band spectrometry with sufficient resolution, information on the cloudy-sky photon path length probability density distribution (briefly called photon path pdf in the following) is drawn from the fact that photons in optically thin and thick spectral interval wavelengths travel on average different long paths during their random cruise in the atmosphere owing to their different probability of being absorbed [e.g., *van de Hulst*, 1980]. In mathematical notation, this leads to a Laplace transformation with the measured intensity ratio $I(\lambda)/I_0(\lambda)$ being the Laplace transform ($\mathcal{L}(k)$) of the desired path length distribution $p(L)$ with respect to the wavelength-dependent and gas density (n)–dependent extinction coefficient ($k(\lambda) = \sigma(\lambda) \cdot n$), where $\sigma(\lambda)$ is the absorption cross section per molecule and n the absorber density. In mathematical terms, we have

$$\frac{I(\lambda)}{I_0(\lambda)} = \mathcal{L}(k) = \int_0^\infty p(L)\, \exp[-k(\lambda)L]\, \mathrm{d}L \qquad (1)$$

where the impact of the dependence of k on pressure and temperature (hence height) is discussed further on. Here, $I(\lambda)$ is the measured intensity and $I_0(\lambda)$ is the extraterrestrial solar intensity. The latter goes back to the work by *Kurucz et al.* [1984] from which residual atmospheric absorption have been removed [*Funk and Pfeilsticker*, 2003].

[1] Institut für Umweltphysik, University of Heidelberg, Heidelberg, Germany.
[2] Space and Remote Sensing Sciences Group, Los Alamos National Laboratory, Los Alamos, New Mexico, USA.
[3] Royal Netherlands Meteorological Institute (KNMI), De Bilt, Netherlands.
[4] Meteorological Institute, University of Bonn, Bonn, Germany.
[5] Now at Meteorological Institute, University of Munich, Munich, Germany.
[6] GKSS Research Centre, Geesthacht, Germany.

0148-0227/06/2004JD005707$09.00

[4] Unfortunately, the inverse Laplace transformation of the measured intensity ratio $I(\lambda)/I_0(\lambda)$ results in a mathematically ill-posed problem since no information is made available by the measurement process on the complex part of the Laplace transformation. This dilemma is frequently resolved by prescribing the mathematical form of the photon path pdf $p(L)$, e.g., by a Gamma, lognormal or any other suitable distribution on the positive real axis normalized to unity.

[5] Another feature of the oxygen A band technique is the information content (IC) of an individual measurement i.e., the number of independent pieces of information that can be drawn from the measurements [i.e., *Stephens and Heidinger*, 2000; *Heidinger and Stephens*, 2000; *Funk*, 2000; *Heidinger and Stephens*, 2002; *Min et al.*, 2004]. These studies revealed that the IC is primarily a function of the out-of-band rejection (OBR) and the spectral resolution of the spectrometer. State-of-the-art instruments are known to provide as much as four independent pieces of information, such as the first 4 moments of the path length distribution, or the first 2 moments and additionally some information the height distribution of the tropospheric aerosol, cloud cover, etc.

[6] A straightforward application of oxygen A band spectrometry is to investigate low-order moments of the photon path length distribution and to relate them to cloud column properties [*Pfeilsticker et al.*, 1998b; *Veitel et al.*, 1998; *Pfeilsticker*, 1999; *Min and Harrison*, 1999; *Min and Clothiaux*, 2003; *Min et al.*, 2004]. In particular, *Pfeilsticker* [1999] investigated the relation of the mean in-cloud photon path $\langle L_c \rangle$ as a function of the rescaled cloud optical depth $\tau_c^* = (1 - g) \cdot \tau_c$, where angular brackets $\langle \cdots \rangle$ denote an average over all paths, τ_c the cloud depth and g the asymmetry factor for Mie scattering. Following the suggestion of *Davis and Marshak* [1997], he found for optically thick cloud covers ($\langle \tau_c^* \rangle \gtrsim 1$) a dependency

$$\langle L_c \rangle \sim \ell_{tr} \times (\tau_c^*)^{\alpha}, \tag{2}$$

where ℓ_{tr} is the rescaled or "transport" photon mean free path (MFP). The so-called Lévy index α in *Pfeilsticker* [1999] data spans the expected range of $1 \leq \alpha \leq 2$, with the precise value depending on the structure of the cloud cover. We refer readers interested in Lévy flights and related topics to *Shlesinger et al.* [1995] and, for applications to fractal clouds, to *Lovejoy and Mandelbrot* [1985].

[7] Likewise, even though not explicitly stated in their study, *Min et al.* [2001] found joint distributions of τ_c (not rescaled) and $\langle L_c \rangle$ (in air mass units) that follow roughly a law in $\langle L_c \rangle / \Delta H \sim (\tau_c)^{\alpha - 1}$ with α in the range 1.4 to 1.7. This is compatible with the above equation (2) since in their Figures 4, 5, 6, and 7 we can identify $\langle L_c \rangle / \Delta H$ with their mean path estimated in air masses, ΔH being the physical thickness of the cloudy part of the atmospheric column, and recalling that $\tau_c^* = \Delta H / \ell_{tr}$.

[8] The regime $\alpha = 2$ is the classical diffusion case where the path length $\langle L_c \rangle$ of photons diffusing via long convoluted random walks through a uniform medium of large rescaled optical depth τ_c^* behaves like $\langle L_c \rangle \sim \ell_{tr} (\tau_c^*)^2$, equivalently $\langle L_c \rangle \sim \Delta H (1 - g) \tau_c$. In sharp contrast, a Lévy index of $\alpha = 1$ describes a predominance of direct (straight) transmission through the "cloud" layer, which is only possible for a negligible small probability of Mie scattering, i.e., clear skies with at most sparse clouds. Accordingly, the diffusion regime $1 \leq \alpha < 2$ is called "anomalous", which *Davis and Marshak* [1997] proposed as a model for paths of photon transmitted by optically thick but inhomogeneous (multilayered and/or broken) cloud covers. More generally, anomalous diffusion by so-called Lévy walks is known to occur for physical entities transported in unlimited (boundary-free) inhomogeneous media. Lévy walks in unlimited media support very large but rare jumps between the visited sites (here, clusters of Mie scattering events inside clouds), which leads to infinite higher-order moments of the path lengths, specifically, moments of the order $\geq \alpha$ [*Samorodnitsky and Taqqu*, 1994]. Because of absorption at the ground and escape at the top of the atmosphere (TOA). The cloudy-sky photon transport can be thought of has having "2.5 dimensions" (i.e., it unfolds in a horizontally infinite but vertically finite medium). Thus Lévy walks confined to a finite slab result [*Buldyrev et al.*, 2001], and these will have finite moments of any order.

[9] In a recent study, *Davis and Marshak* [2002] revisited the problem of classical ($\alpha = 2$) diffusion through a homogeneous optically thick slab. Therein they provided full analytical expressions for the first two moments $\langle L_c \rangle$ and $\sqrt{\langle L_c^2 \rangle}$ as a function of the slab (cloud) vertical extension ΔH and optical depth τ_c. These relations for classical diffusion are tested in our study, in particular, as to whether they hold true for real cloud covers (hence Lévy indices $\alpha < 2$).

[10] Accordingly the study is organized as follows. Section 2 describes the employed methods in our observations. Section 3 reports on the observation. Section 4 discusses the theoretical relations between cloud properties and photon paths. Section 5 discusses our results with respect to the theoretical information in the *Davis and Marshak* [1997, 2002] studies, and section 6 concludes our study with the wider implications for photon transport in cloudy skies.

2. Methodology

[11] Pertinent experimental information has already be summarized in recent work dealing with our oxygen A band instrument and the employed method [*Platt*, 1994; *Platt and Stutz*, 2004; *Harrison and Min*, 1997; *Pfeilsticker et al.*, 1998b; *Pfeilsticker*, 1999; *Funk and Pfeilsticker*, 2003]; thus only the most salient aspects are described here. The method to infer the photon path pdf of solar photons transmitted through to the ground relies on high-resolution differential optical absorption spectroscopy (DOAS) of the oxygen A band (760–780 nm) in zenith scattered skylight [*van de Hulst*, 1980; *Harrison and Min*, 1997; *Pfeilsticker et al.*, 1998b]. The main attributes of our technique are (1) a reasonably high spectral resolution in order to resolve individual oxygen A band lines, a feature which is necessary in order to maximize the information content retrievable from the measured spectra [*Heidinger and Stephens*, 2000; *Stephens and Heidinger*, 2000; *Funk and Pfeilsticker*, 2003; *Min et al.*, 2004]; (2) a large photon detection sensitivity leading to a high signal-to-noise ratio (SNR), $\geq$1000, that can be achieved within a reasonably short integration time ($\approx$10 s); and (3) a small field of view (FOV) in order to probe the path pdf within horizontal

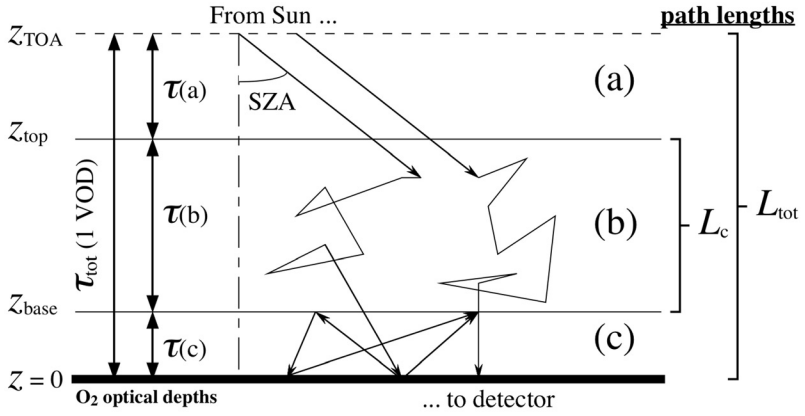

Figure 1. A schematic of the three atmospheric regions of interest. In region a the solar rays are slant but not scattered. In region b, clouds are present and scattering occurs. In region c the scattered light ultimately reaches the spectrometer often directly from the base of the lowest cloud, occasionally after one or more reflections of the ground and the clouds. Here we illustrate only the simple model where beams are reflected at the cloudy region's lower boundary. See text for a quantification of this effect and a more advanced model where light reflected from the ground can penetrate the cloudy region.

scales smaller than the radiative smoothing scale typical for the cloud cover [*Marshak et al.*, 1995; *von Savigny et al.*, 1999].

2.1. Instrument

[12] The deployed instrument consists of three major parts: (1) a light intake (entrance optics) that provides a FOV = 0.86° from which the light is directed into (2) a blazed-grating UHRS Sopra F1500 spectrometer operated in seventh order to image the spectral interval 767.7–770.7 nm at a full width, half maximum (FWHM) of 0.0135 nm for a 70 μm wide entrance slit, and (3) a light detection system consisting in a front-illuminated CCD camera manufactured by Andor (type DU440-UV with a Marconi EEV CCD 42-10 chip cooled to −50°C and read out by a 1 MHz controller card). Because of the size of the spectrometer with an optical axis in the horizontal, the light intake optics consist of a 45° mirror mounted into the knee of an L-shaped tube through which the zenith scattered skylight is observed with a f/13.5 FOV. The spectrometer is surrounded by a thermally stabilized box (at 30°C) in order to keep the optical imaging constant. The CCD chip provides a well depth of 600000 e^-/pixel, a dark current of 0.03 e^-/pixel/s at −50°C and a readout noise of 2.4 e^-/pixels. By coadding 400 pixel lines in a single scan which are illuminated within 2 s, the noise (15492 e^-) is dominated by photoelectron noise. Accordingly, for a fully saturated spectrum, a maximum SNR ≈ 15000 can be achieved, but in practice SNR is somewhat lower for optical dense wavelengths since less light is received there. The whole instrument is mounted into a portable container laboratory for shipment to measurements sites.

2.2. Retrieval Method

[13] The measured oxygen A band spectra $I(\lambda)$ are evaluated in an iterative least squares fitting process which minimizes the differences of the measured to a modeled $I_{mod}(\{a\}; \lambda)$: $\chi^2 = [I(\lambda) - I_{mod}(\{a\}; \lambda)]^2 \rightarrow min$ [*Funk and Pfeilsticker*, 2003] by varying the model's free parameters represented by the set $\{a\}$. The modeled spectrum is defined (1) by a convolution integral over all wavelengths of the instrument's slit function $S(\lambda - \lambda')$ with the predicted spectral radiance based on (2) a high resolution TOA solar spectrum $I_0(\lambda)$ [*Kurucz et al.*, 1984] (from which residual atmospheric oxygen band absorption has been removed) modulating the integral over the appropriately nondimensionalized path length L of (3) prescribed photon path pdf for the cloud-free part from cloud top to the Sun (region a), in cloud-photon path (region b), and the path between cloud bottom and the ground times (region c), and (4) the Lambert-Beer exponentials of integrals of forwardly calculated oxygen A band absorption coefficients $k(\lambda; T_j, p_j)$ on $j = 1, \ldots, 40$ atmospheric levels (with vertical extensions Δz_j) for which actually measured atmospheric profiles of $T(z)$ and $p(z)$, $0 \le z \le z_{TOA}$, are used as input. For the calculation of the oxygen A band absorption cross sections going into the calculations of the layer extinction $k(\lambda; T(z), p(z))$, line strengths and broadening parameters from HITRAN-2000 [*Rothman et al.*, 2003] are used and Voigt-type line profiles are assumed. For each observation, the following partial photon path pdfs are prescribed for the three atmospheric regions (a, b, and c), as illustrated in Figure 1.

[14] 1. For region a the oxygen A band absorption is calculated using ray tracing for the known solar zenith angle (SZA) and the measured (T, p) profile; here a delta pdf is assumed for $p(\{a\}; L)$ and no parameter is required.

[15] 2. Likewise, the correction for absorption in region c is calculated for the mean of the photon pdf (see below) allowing nonetheless for multiple reflections between ground (albedo $A_g \approx 0.35$, for vegetation at 760 nm) and cloud (albedo R_c, estimated approximately from τ_c^* in equation (15) below).

[16] 3. Finally for region b, $p(\{a\}; L_c)$ is taken to be a Gamma distribution, where the only parameters in the set $\{a\}$ are the in-cloud mean photon path $\langle L_c \rangle$ and its variance $\langle L_c^2 \rangle$.

[17] Note that the random in-cloud photon paths $\langle L_c \rangle$ and its variance $\langle L_c^2 \rangle$ and all geometrical lengths, such as, for example, the cloud vertical extension ΔH are expressed in

their natural nondimensional units or VODs (standing for "vertically integrated oxygen density"). More precisely, we start by defining the oxygen path length (unit VOD) between atmospheric levels z_1 and z_2

$$L(z_1, z_2) = \int_{z_1}^{z_2} n(z)\,\mathrm{d}z \;/\; \int_0^{\infty} n(z)\,\mathrm{d}z \tag{3}$$

where oxygen density is calculated from the ideal gas law ($n(z) = 0.21 \cdot p(z)/k_B T(z)$). Next we define the optical path length between z_1 and z_2

$$\tau_{O_2}(\lambda; z_1, z_2) = \int_{z_1}^{z_2} k(\lambda; T(z), p(z))\, n(z)\,\mathrm{d}z \tag{4}$$

[18] Then, knowing the altitudes of cloud base (z_{base}) and cloud top ($z_{top} = z_{base} + \Delta H$) from lidar and/or cloud radar, we can compute specifically the following optical paths:

$$\begin{aligned}
\tau_{col}(\lambda) &= \tau_{O_2}(\lambda; 0, z_{TOA}) \\
\tau_{(a)}(\lambda) &= \tau_{O_2}(\lambda; z_{top}, z_{TOA}) / \cos(SZA) \\
\tau_{(b)}(\lambda) &= \tau_{O_2}(\lambda; z_{base}, z_{top}) \\
\tau_{(c)}(\lambda) &= \tau_{O_2}(\lambda; 0, z_{base}) \times \left(1 + \frac{5A_g R_c}{1 - A_g R_c}\right)
\end{aligned} \tag{5}$$

Here the first and third are straightforward the vertical paths, while the second and fourth are respectively slant and more complex paths (see below).

[19] The last expression for the oxygen path cumulated below the cloud needs some more discussion. We have displayed explicitly a correction term for multiple ground/cloud base reflections. It is estimated with a summed geometric series in $A_g R_c < 1$ multiplying twice the hemispherical flux-weighted mean of the cosecant (which is 2) for both downward and upward path, plus one more VOD for region c to get straight back down into the instrument; in summary, letting $\mu = \cos(ZA)$ the correction is indeed

$$\left(2 \times \frac{\int_0^1 (1/\mu)\mu\mu}{\int_0^1 \mu\mu} + 1\right) \sum_{N \geq 1} (A_g R_c)^N = \frac{5A_g R_c}{1 - A_g R_c}.$$

Using $R_c \approx 0.6$ and $A_g = 0.35$, we find a correction term of about unity, but this multiplies a relatively small part of the VOD. In our observations, z_{base} is at the most about 1/4 of a vertical scale height (≈8 km); hence in our units $\tau_{(c)}(\lambda; 0, z_{base}) \lesssim 0.25$ VOD, a small value when compared to the inferred values (see section 2.3).

[20] In a good approximation, our measured radiances are then given by the following forward model

$$\begin{aligned}
I_{mod}(\{a\}; \lambda) = \int_{-\infty}^{+\infty} & S(\lambda - \lambda') \cdot I_0(\lambda') \\
& \cdot \exp\left[-\tau_{(a)}(\lambda') - \tau_{(c)}(\lambda')\right] \\
& \times \left\{ \int_0^{\infty} \exp\left[-\tau_{(b)}(\lambda') L_c\right] \cdot p(\{a\}; L_c) \cdot \mathrm{d}L_c \right\} \cdot \mathrm{d}\lambda'
\end{aligned} \tag{6}$$

where the integral in L_c is taken analytically, given the prescribed expression for $p(\{a\}; L_c)$. This way, the random in-cloud photon path L_c is expressed in the desirable nondimensional units (VOD for the cloudy region). Its value can thus be directly with theoretical predictions for $L_c/\Delta H$. Finally, the spectral retrieval yields the total paths $\langle L_{tot} \rangle$ and $\langle L_{tot}^2 \rangle$ from the inferred $p(\{a\}; L_c)$ as nondimensional random variables.

[21] For the retrieval of reliable path pdfs using the oxygen A band method, however, one needs to consider carefully the following characteristics of individual measurements: (1) the instrumental slit function, $S(\lambda - \lambda')$ since it is known to show a large sensitivity on the inferred path pdf [e.g., *Funk and Pfeilsticker*, 2003] (in our study the slit function is monitored by the He/Ne laser line at 663 nm in Figure 2 and the line shapes of the solar Fraunhofer lines observed in the spectral interval under consideration), (2) the resolving power of the spectrometer, and (3) the OBR from Figure 2 since together with the former characteristic it largely determines the possible number of independent parameters (the size of the set $\{a\}$) that can be determined in a spectral retrieval [e.g., *Stephens and Heidinger*, 2000; *Heidinger and Stephens*, 2000, 2002; *Funk*, 2000; *Min et al.*, 2004].

[22] In agreement with recent considerations by *Min et al.* [2004], the values of the relevant parameters (spectral resolution FWHM = 0.0135 nm, OBR (10^{-4}) indicate that our measurements allows us to infer four independent pieces of information, i.e., parameters a_i with $i = 1, \ldots, 4$. In the present study, only two pieces of independent information are generally used, specifically, the first two moments of the assumed photon path pdf. If not otherwise stated, Gamma-type path pdfs are assumed in the evaluation procedure [*Funk*, 2000] since they are known to reflect accurately photon path pdf for cloud covers that can be modeled as a single plane-parallel layer [*van de Hulst*, 1980] and, for all other types of cloud covers, they may be regarded as reasonable approximations for more complicated path pdf shapes [*Funk and Pfeilsticker*, 2003].

[23] Figure 3 shows a typical example of measured and simulated oxygen A band spectra (Figure 3, top), the log of the ratio of the two spectra taken as the residual of the retrieval in equivalent optical path (Figure 3, middle), and the inferred photon path pdf assuming a Gamma-type distribution (Figure 3, bottom). The observed spectrum was obtained at Cabauw (NL) on 11 May 2003 at 1459 UT (see marker on Figure 4) when the solar zenith angle (SZA) was 52.25°. Although some regular features remain in the residual which are due primarily to an etaloning on the CCD chip, the peak-to-peak residual ($5 - \sigma$) is ≤ 0.01. This result indicates that throughout the whole spectrum SNR ≥ 200, a result being in agreement with the theoretical considerations of *Stutz and Platt* [1996]. Further sensitivity tests of inferred and simulated path pdf indicate that, for SNR ≥ 200 and by assuming Gamma-type path pdf for not too complicated cloud covers (i.e., well-layered clouds), the first two moments of the path pdf can be determined to about ±5%. Accordingly, in the following, the varying uncertainties on the inferred path pdfs are estimated by seeing how the residuals of the spectral fitting process propagate into the values of the inferred first two moments of the path pdf.

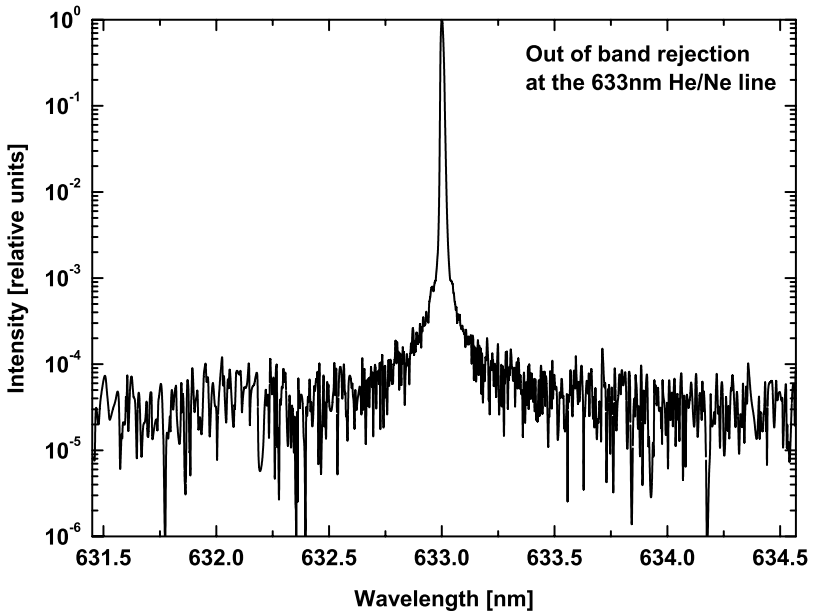

Figure 2. Measured out-of-band rejection (OBR) for the He/Ne line at 633 nm. The OBR reaches values $<10^{-4}$ for wavelengths 6 FWHM off the line center.

2.3. Total Atmospheric and In-Cloud Path

[24] Finally, in order to relate inferred $\langle L_{\mathrm{tot}}\rangle$ and $\langle L_{\mathrm{tot}}^2\rangle$ to the in-cloud path length $\langle L_{\mathrm{c}}\rangle$ and $\langle L_{\mathrm{c}}^2\rangle$, we need to consider the following individual contributions to both moments of the total atmospheric path.

[25] 1. Evidently for region a, above clouds, photon path length are δ-function distributed, and hence we obtain

$$\langle L_{\mathrm{above}}\rangle = \sqrt{\langle L_{\mathrm{above}}^2\rangle} = L\big(z_{\mathrm{top}},\infty\big)/\cos(SZA) \tag{7}$$

[26] 2. As before for region c, below cloud, we consider multiple ground/cloud base reflection, and accordingly arrive at

$$\langle L_{\mathrm{below}}\rangle = \sqrt{\langle L_{\mathrm{below}}^2\rangle} = L(0,z_{\mathrm{base}}) \times \left(1+\frac{5A_{\mathrm{g}}R_{\mathrm{c}}}{1-A_{\mathrm{g}}R_{\mathrm{c}}}\right) \tag{8}$$

[27] 3. Next, we consider the contribution to the total path (not illustrated in Figure 1) from radiation reflected at the ground that penetrates into the cloud bottom and after multiple reflection returns to the ground. *Davis et al.* [1999] already dealt with the problem motivated by cloud lidar studies. Neglecting preasymptotic corrections, the result is

$$\langle L_{\mathrm{refl}}\rangle \approx 2\chi \times L\big(z_{\mathrm{base}},z_{\mathrm{top}}\big) \tag{9}$$

with $\chi = 0.7014$ [*Case and Zweifel*, 1967]. We note that is expression is for homogeneous cloud layers, but this should be good enough for a correction. Also, *Davis et al.* [1999] find a different expression than above for $\sqrt{\langle L_{\mathrm{refl}}^2\rangle}$, but again we will not be concerned with this difference since all we are doing here is a correction.

[28] Finally, we use simple relations between $\langle L_{\mathrm{tot}}\rangle$, $\langle L_{\mathrm{tot}}^2\rangle$ and $\langle L_{\mathrm{c}}\rangle$, $\langle L_{\mathrm{c}}^2\rangle$, respectively, when the random variables have a constant difference based on a weighted sum (relative to the skylight transmitted from the cloud bottom) of all contributions. For the first moment, we have

$$\langle L_{\mathrm{tot}}\rangle = \langle L_{\mathrm{c}}\rangle + \langle L_{\mathrm{above}}\rangle + \langle L_{\mathrm{below}}\rangle + \langle L_{\mathrm{refl}}\rangle \times \frac{A_{\mathrm{g}}}{1-A_{\mathrm{g}}R_{\mathrm{c}}}$$

where the last weighting originates with the same sequence of double ground-cloud reflections as summed above. For the second moment, we simply express that is no new variance (only a deterministic shift) exists at the present level of modeling for corrections due to ground-reflected radiation, and hence we obtain

$$\langle L_{\mathrm{c}}^2\rangle = \langle L_{\mathrm{c}}\rangle^2 + \langle L_{\mathrm{tot}}^2\rangle - \langle L_{\mathrm{tot}}\rangle^2.$$

To illustrate the magnitudes of all contributions, the following values are obtained from the oxygen A band spectrometry and ancillary data for the observation on 11 May 2003, 1459 UT (Figure 4): $\langle L_{\mathrm{tot}}\rangle = 2.165$ VOD, $\langle L_{\mathrm{tot}}^2\rangle = 5.94$ VOD^2, $z_{\mathrm{base}} = 1950$ m (0.78 VOD), $z_{\mathrm{top}} = 5400$ m (0.51 VOD), hence $\Delta H = 3450$ m (0.27 VOD), $\tau_{\mathrm{c}}^* = 2.2$, and SZA = 52.25°. Accordingly, we obtain $\langle L_{\mathrm{above}}\rangle = \sqrt{\langle L_{\mathrm{above}}^2\rangle} = 0.832$ VOD, $\langle L_{\mathrm{below}}\rangle = \sqrt{\langle L_{\mathrm{below}}^2\rangle} = 0.504$ VOD, $\langle L_{\mathrm{refl}}\rangle = 0.385$ VOD, hence $\langle L_{\mathrm{c}}\rangle = 0.659$ VOD and $\langle L_{\mathrm{c}}^2\rangle = 1.687$ VOD^2.

3. Observations

[29] In our study we report on photon path pdf data inferred from oxygen A band measurements that were taken within the framework of the BBC-1 and -2 field programs (Baltex Bridge Campaign, Phases 1 and 2) at Cabauw in the Netherlands (51.9703°N, 4.9262°E) during September 2001 and May 2003. Our contribution came through the BMBF-sponsored AFO2000 4D-clouds project. Detailed information on the BBC-1/2 campaigns and the 4D-clouds project are provided at http://www.knmi.nl/samenw/bbc2/ and http://www.meteo.uni-bonn.de/projekte/4d-clouds/ and in a

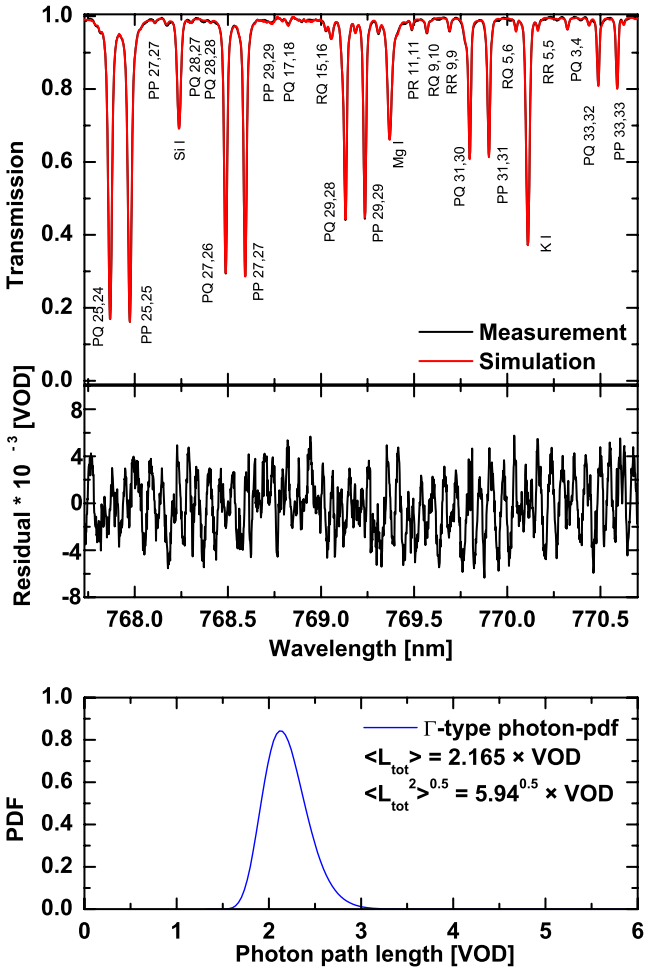

Figure 3. (top) Comparison of measured (black) and simulated (red) oxygen A band spectrum for the observation at Cabauw (NL) on 11 May 2003 at 1459 UT. The identification of the oxygen A band and solar Fraunhofer lines is given next to the line. (middle) Residual spectrum taken as the natural log of the ratio of measured and simulated spectrum, hence the natural units of vertically-integrated optical density (VOD), or air mass. (bottom) Inferred photon path pdf, assuming a Γ distribution for the in-cloud transfer.

recent publication by *Crewell et al.* [2004]. During both campaigns, our oxygen A band measurements were supported by simultaneous measurements of a large number of ground-based, in situ, and aircraft-based instruments, which all aim at a thorough characterization of the physical properties of investigated cloud cover and its interaction with the atmospheric radiation.

[30] Most important here are the measurements of the cloud vertical structure of the 35 GHz radar operated by KNMI and the "Miracle" 95 GHz radar cloud radar from the Institute of Coastal Research at the GKSS Research Center [*Donovan et al.*, 2001; *Quante et al.*, 2000], and of the liquid water path (LWP) microwave instruments MICCY (Microwave Radiometer for Cloud Cartography) from the University of Bonn [*Crewell et al.*, 2001] and RPG-HATPRO (humidity and temperature profiler) from Radiometer Physics GmbH (RPG) [*Rose et al.*, 2005].

[31] Figures 4, 5, and 6 display the measured mm cloud radar reflectivity, liquid water path (LWP) and the inferred mean $\langle L_{tot}\rangle$ and root-mean-square (RMS) $\sqrt{\langle L_{tot}^2\rangle}$ of the atmospheric photon paths for the measurements at Cabauw on 23 September 2001 and 11 and 22 May 2003. Figures 4 (bottom), 5 (bottom), and 6 (bottom) nicely demonstrate how the measured LWP, the occurrence of clouds as detected by the radar, and the inferred $\langle L_{tot}\rangle$ and $\sqrt{\langle L_{tot}^2\rangle}$ correlate strongly with each other, a finding largely in agreement with results from previous studies [*Min and Harrison*, 1999; *Funk and Pfeilsticker*, 2003; *Min et al.*, 2004]. This shows the increase in (mean) photon path lengths for solar photons being transmitted through the cloud cover via increased numbers of multiple Mie scattering events because of the increased LWP. However, why $\langle L_{tot}\rangle$ and $\langle L_{tot}^2\rangle^{1/2}$ track each other so closely is not evident, especially in the more complex cloud scenarios.

[32] The theoretical relationships among the photon path length statistics within the cloud (that we denote $\langle L_c\rangle$ and $\langle L_c^2\rangle$), LWP, vertical extension of clouds (ΔH), and type of cloud cover, are discussed in the next section in more detail.

4. Cloud Properties and Photon Paths

[33] We elaborate here on some theoretical relations among $\langle L_c\rangle$, $\sqrt{\langle L_c^2\rangle}$, LWP, τ_c, ΔH, and cloud type. We will then discuss in the next section our findings with respect to this knowledge. For this purpose, we first recall some basic cloud equations and their relation to the radiative (RT) formulated in terms of photon path statistics.

4.1. Cloud Optical Depth

[34] We first define the cloud optical depth τ_c as

$$\tau_c = \frac{\Delta H}{\ell_{Mie}} \tag{10}$$

where ℓ_{Mie} is the mean free path for the Mie scattering by cloud droplets and possibly also by aerosol (we can neglect Rayleigh scattering at 770 nm).

[35] Furthermore, with the ΔH definition given above, the Mie scattering length scale ℓ_{Mie} should be regarded as an "effective" Mie scattering length scale for the atmospheric column that stretches from the lowest to the uppermost atmospheric layers containing clouds. It is thus calculated from equation (10) with known ΔH (from radar, even if there are gaps between clouds and/or layers) and known cloud optical depth τ_c (from passive microwave radiometry yielding LWP and, typically, an assumption about droplet size).

4.2. Transport Mean Free Path

[36] This definition of τ_c allows us to define a rescaled mean free path $\ell_{tr} = \ell_{Mie}/(1-g)$ [e.g., *Davis et al.*, 1997a] and accordingly a rescaled cloud optical depth τ_c^*

$$\tau_c^* = (1-g)\cdot\frac{\Delta H}{\ell_{Mie}} = (1-g)\cdot\tau_c \tag{11}$$

The rescaled cloud optical depth accounts for the fact that Mie scattering largely favors forward scattering. Further since in our study we mostly address the RT in liquid water

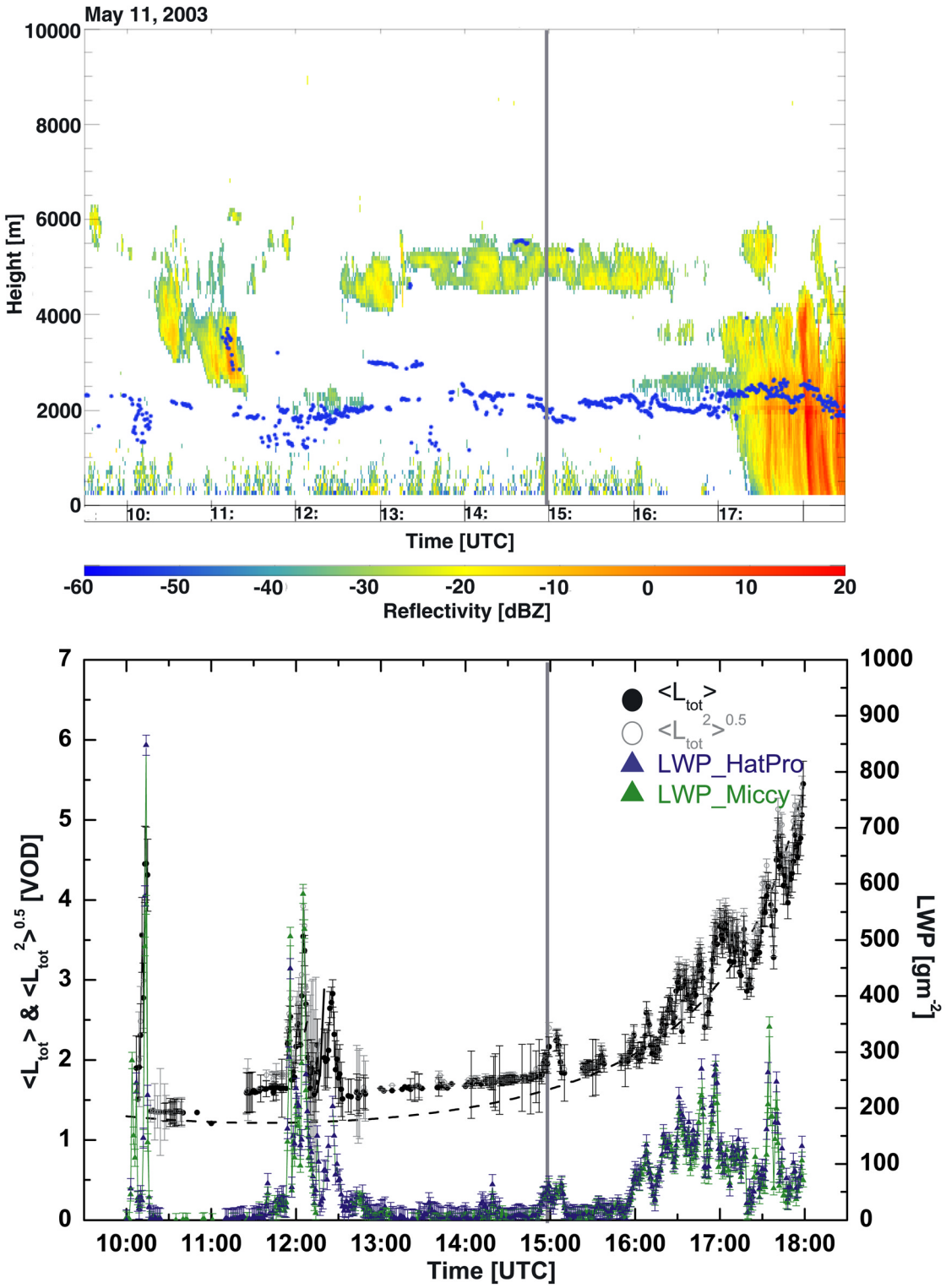

Figure 4. (top) Radar reflectivity measured by the KNMI 35 GHz radar at Cabauw (NL) on 11 May 2003 between 1000 and 1800 UT. The blue dots indicate the cloud bottom measured from the KNMI ceilometer. For this day the cloud cover is characterized by low-level and midlevel clouds (Sc, St1, and St2) between 2000 and 6000 m. (bottom) Time series of inferred first two moments of the photon paths ($\langle L_{\mathrm{tot}} \rangle$ and $\sqrt{\langle L_{\mathrm{tot}}^2 \rangle}$) in VOD units of the oxygen atmospheric column (left ordinate axis) and liquid water path (LWP, right ordinate axis) measured by MICCY and by HATPRO. The black dashed line shows the photon path lengths for the direct sunlight 1/cos (SZA). A marker indicated the raw observations displayed analyzed in Figure 3.

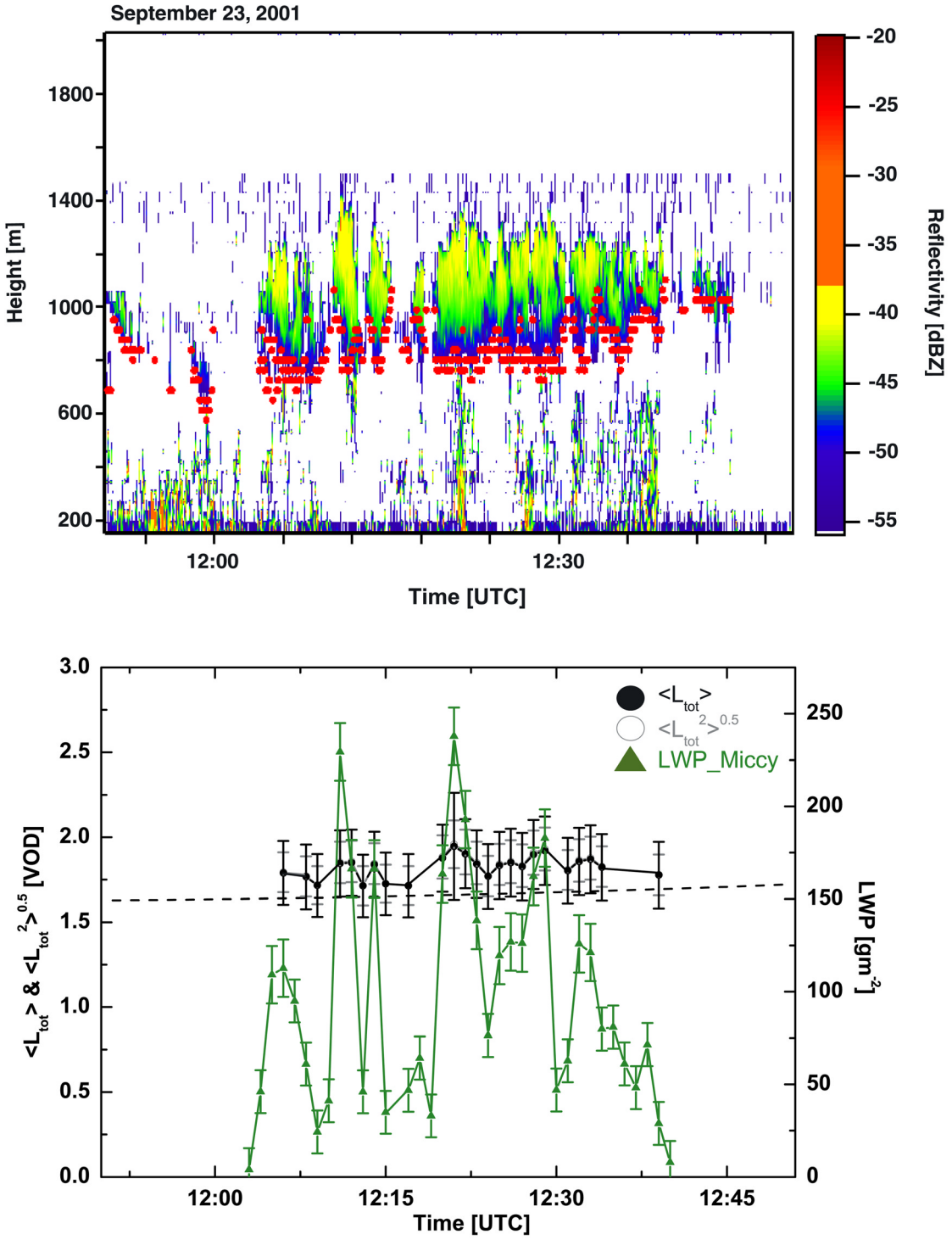

Figure 5. (top) Radar reflectivity measured by the by the GKSS 95 GHz radar at Cabauw (NL) on 23 September 2001 between 1152 and 1248 UT. The red dots indicate the cloud bottom measured from the KNMI ceilometer. The cloud cover is characterized by a broken-in place continental Sc deck, extending from 1000 to 1600 m above sea level (ASL). (bottom) Time series of inferred first two moments of the photon paths ($\langle L_{\mathrm{tot}} \rangle$ and $\sqrt{\langle L_{\mathrm{tot}}^2 \rangle}$) in VOD units of the oxygen atmospheric column (left ordinate axis) and liquid water path (LWP, right ordinate axis) measured by MICCY. The black dashed line shows the photon path lengths for the direct sunlight 1/cos(SZA).

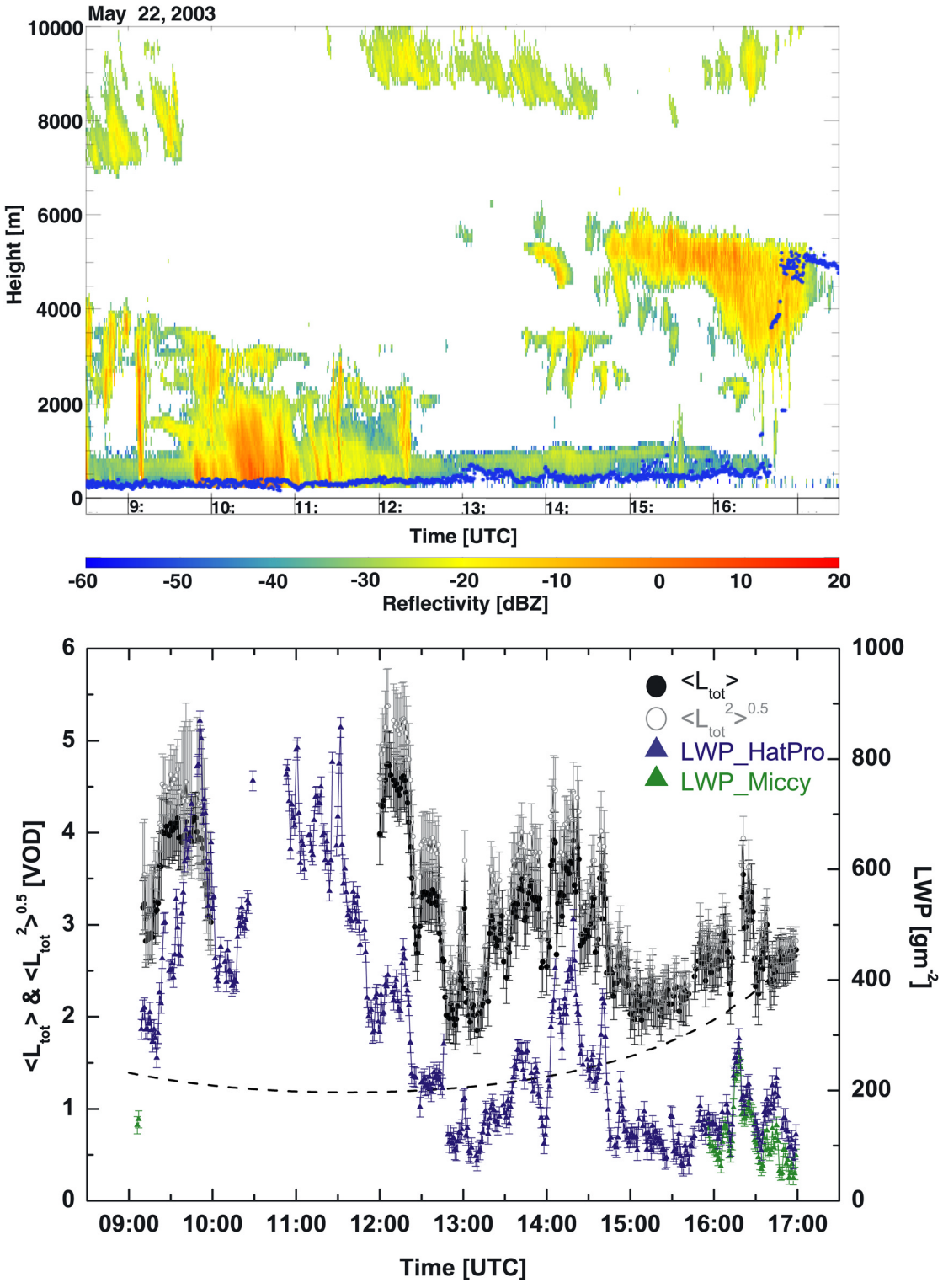

Figure 6. (top) Radar reflectivity measured by the KNMI 35 GHz radar at Cabauw (NL) on 22 May 2003 between 0830 and 1730 UT. The blue dots indicate the cloud bottom measured from the KNMI ceilometer. For this day the cloud cover is characterized by low-level clouds (Sc, St1, and St2) below 4000 m and some midlevel (As) and high-level Cc clouds occurring occasionally between 3000 and 6000 m and 7000 and 10,000 m, respectively. (bottom) Time series of inferred first two moments of the photon paths ($\langle L_{\mathrm{tot}} \rangle$ and $\sqrt{\langle L_{\mathrm{tot}}^2 \rangle}$) in VOD units of the oxygen atmospheric column (left ordinate axis) and liquid water path (LWP, right ordinate axis) measured by MICCY and by HATPRO. The black dashed line shows the photon path lengths for the direct sunlight 1/cos(SZA).

clouds, the asymmetry factor g for Mie scattering attains a value of $g = 0.85$. Accordingly, it takes on the average 6 to 7 scattering events in liquid water clouds before the incoming light as all but "forgotten" its initial direction of incidence.

4.3. Liquid Water Path and Rescaled Cloud Optical Depth

[37] Next, we recall the well-known relations among the effective cloud droplet radius r_e, the liquid water content (LWC), the number of droplets $dN(r)$ per (infinitesimal) radius interval dr ($n(r) = dN/dr$) and ℓ_{Mie}. First, we have

$$r_e = \frac{\int_0^\infty r^3 \cdot n(r)dr}{\int_0^\infty r^2 \cdot n(r)dr} = \frac{\int_0^\infty r^3 \cdot dN(r)}{\int_0^\infty r^2 \cdot dN(r)} = \frac{\overline{r^3}}{\overline{r^2}}. \quad (12)$$

From the numerator, we can deduce LWC = $(4\pi/3)\,\overline{r^3}\rho_w N$ where ρ_w is the density of liquid water and N is the total droplet density. From the denominator, we can deduce $1/\ell_{Mie} = 2\pi\overline{r^2}N$ in the limit of large size parameters in Mie scattering theory. Therefore, by elimination of the moments of r in (12) we obtain

$$\ell_{Mie} = \frac{2 \cdot r_e \cdot \rho_w}{3 \cdot LWC} \quad (13)$$

Noteworthy here is that in general LWC and r_e (and thus ℓ_{Mie}) are functions of the spatial coordinates x, y, and z (see below), but in the following we skip its dependency in the vertical coordinate since we are mostly interested in the vertical column-averaged quantities of the mean path length $\langle L_c \rangle$, and the liquid water path LWP. Using the column integrated liquid water path $LWP = \int_{z_1}^{z_2} LWC(z) \cdot dz = \overline{LWC} \cdot (z_2 - z_1) = \overline{LWC} \cdot \Delta H$, we obtain from equations (11) and (13) that

$$\tau_c^* = (1-g)\,\tau_c = (1-g) \times \frac{3 \cdot LWP}{2 \cdot r_e \cdot \rho_w} \quad (14)$$

which relates the effective cloud optical depth τ_c^* to the measurable quantity LWP.

4.4. Classical Photon Diffusion

[38] Intuitively speaking, classical photon diffusion occurs in optically thick media ($\tau_c^* \gtrsim 1$) where the photons are transported by long convoluted random walks. In cloud optics, this scenario materializes in "homogeneous" cloud covers (i.e., stratiform cloud decks) where variability-induced changes in the domain average radiative fluxes are effectively smeared-out by Mie scattering. Arguably, this is the case on spatial scales smaller than the radiative smoothing scales based on reflection $\approx\sqrt{\ell_{tr} \cdot \Delta H} = \Delta H/\sqrt{\tau_c^*}$ [*Marshak et al.*, 1995; *Davis et al.*, 1997a], or on transmission $\approx \Delta H$ [*von Savigny et al.*, 1999; *Davis and Marshak*, 2002]. However, the best estimate so far is the characteristic scale of the exponential decay of the spatial Green function $\Delta H/\pi R_c(\tau_c^*)$ [*Polonski and Davis*, 2004] where R_c is cloud albedo, given by

$$R(\tau_c^*) = 1/(1+\epsilon)$$
$$\epsilon(\tau_c^*) = \frac{T}{R} = \frac{2\chi}{(1-g)\tau_c} = \frac{2\chi}{\tau_c^*}. \quad (15)$$

This last quantity becomes small as τ_c^* becomes large. Here, $T = 1 - R$ is transmittance and the value of χ is often taken to be 2/3 although $0.7104\cdots$ is the proper answer for the benchmark Milne problem [*Case and Zweifel*, 1967]. Conversely, cloud variability on spatial scales larger than these smoothing scales can be resolved with the novel instrumentation at hand, i.e., with the more sensitive oxygen A band spectrometer than previously used.

[39] *Davis and Marshak* [2002] recently investigated of classical diffusion through a homogeneous slab: sources (assumed diffuse) on one side, and detectors (for flux) on the other. Applying Green's function analysis to diffusive transport through a conservatively scattering homogeneous slab of geometric thickness ΔH for $\tau_c^* \gtrsim 1$, the authors inferred the following relations for the first two moments of the photon path lengths: For the first moment, $\langle L_c \rangle$,

$$\langle L_c \rangle / \Delta H = \frac{1}{2} \cdot \tau_c^* \cdot [1 + C_1(\epsilon)]$$
$$C_1(\epsilon) = \frac{\epsilon}{2} \cdot \frac{4 + 3\epsilon}{1 + \epsilon}. \quad (16)$$

For the second moment, $\langle L_c^2 \rangle$,

$$\langle L_c^2 \rangle / \Delta H^2 = \frac{7}{20} \cdot (\tau_c^*)^2 \cdot [1 + C_2(\epsilon)] \quad (18)$$

$$C_2(\epsilon) = \frac{\epsilon}{14} \cdot \frac{56 + 166\epsilon + 150\epsilon^2 + 45\epsilon^3}{(1+\epsilon)^2}. \quad (19)$$

Succinctly, classical diffusion theory predicts that $\langle L_c \rangle / \Delta H \sim \tau_c^*$ and that $\langle L_c^2 \rangle^{1/2} / \Delta H$ is also $\sim \tau_c^*$. The ratio of the prefactors for $\langle L_c^2 \rangle^{1/2} / \langle L_c \rangle$ is $\sqrt{7/5} \approx 1.18$ for $\tau_c^* \gg 1$, when the correction terms vanish. Although diffusion is not expected to be a valid transport theory when $\tau_c^* < 1$, that limit leads to $\langle L_c^2 \rangle^{1/2} / \langle L_c \rangle \approx \sqrt{2}$. Therefore the moment ratio varies only modestly over the full range of optical depths.

4.5. Anomalous Diffusion

[40] In order to account for cloud inhomogeneities (on scales larger than described above) and the patchiness of the cloud cover, *Davis and Marshak* [1997] suggested that anomalous diffusion, i.e., truncated Lévy walks, would give a better representation of the cloudy-sky photon transport. Lévy distributed path pdfs result from power law distributed step sizes between individual (Mie) scattering events with the characteristic exponent being $-(\alpha + 1)$. A truncated Lévy walk will then occur for photons transported through a (vertically and/or horizontally) "patchy" cloud cover and eventually absorbed at the ground, or returned to space. The truncation also leads to the existence of moments all orders, recalling that moments of order $\geq\alpha$ are infinite for unbounded Lévy walks.

[41] As stated in section 1, the Lévy walk model predicts for the mean photon path $\langle L_c \rangle \sim \Delta H \cdot (\tau_c^*)^{\alpha-1}$ for $1 \leq \alpha \leq 2$ [*Davis and Marshak*, 1997; *Buldyrev et al.*, 2001]. The upper limit ($\alpha = 2$) reverts to the above case of classical diffusion in equation (16). The second and higher-order moments of the path pdfs have not yet been investigated theoretically for Lévy transport, neither for the scaling exponents nor for the prefactors nor the preasymptotic correction terms given in equations (16) and (18) for $\alpha = 2$. Notwithstanding, in the following discussion, we

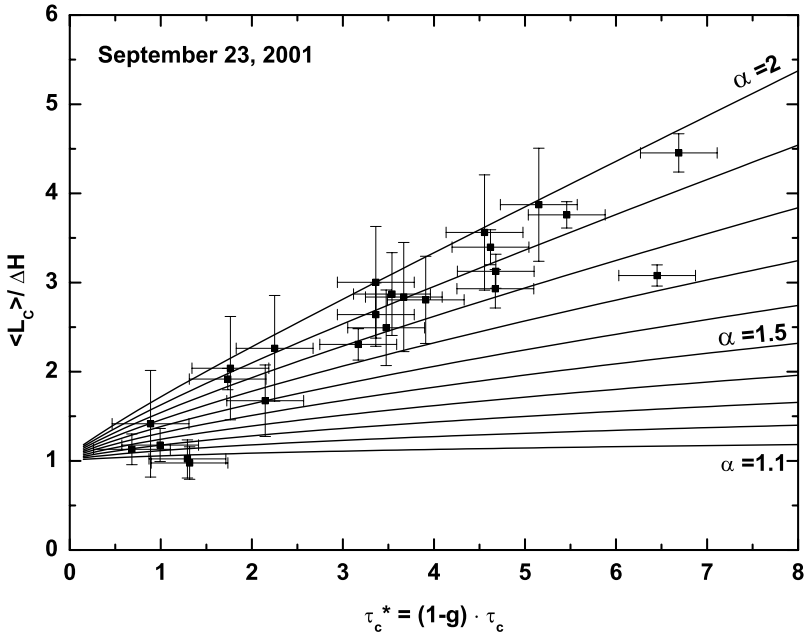

Figure 7. Mean cloud photon paths $\langle L_c \rangle$ as a function of effective cloud optical depth τ_c^* for the 23 September 2001 observation. The lines are predictions based on equation (16) modified as explained in the text for different values of the Lévy exponent $\alpha \leq 2$.

generalize equations (16) and (18) simply by taking the right-hand sides of equations (16) and (18), respectively, to the powers $(\alpha - 1)$ and $2 \cdot (\alpha - 1)$. This implies in particular that the ratio $\sqrt{\langle L_c^2 \rangle}/\langle L_c \rangle$, which is $\sqrt{7/5} \cdot [1 + C_2(\tau_c^*)]^{1/2}/[1 + C_1(\tau_c^*)] \in (1.18, 1.41]$ for $\alpha = 2$, will vary even less (at slightly lower values) for $1 < \alpha < 2$.

[42] That is the straightforward hypothesis that we examine with our new field data for $\langle L_c \rangle$, $\langle L_c^2 \rangle$, and τ_c^* in the next section.

5. Results and Discussion

[43] We now investigate the validity of the modified equations (16) and (18) by inspecting (1) the inferred mean path length $\langle L_c \rangle$ as a function of τ_c^* and (2) the ratio of the inferred RMS and mean photon paths $\sqrt{\langle L_c^2 \rangle}/\langle L_c \rangle$ (Figure 7, 8, 9, 10, 11, and 12). For the calculation of τ_c^* from measured LWP and ΔH, an asymmetry value g of 0.85 was assumed and a constant effective radius of $r_e = 8$ μm (±1 μm) was taken. The latter value is inferred from tethered balloon r_e measurements up to 1500 m altitude that were conducted during the campaign [*Schmidt et al.*, 2004; *Crewell et al.*, 2004].

[44] Figures 7, 9, and 11 demonstrate that the effective Lévy index α of our modified model attains all values between 1 and 2, whereby the limiting case $\alpha = 2$ (classical diffusion) occurs only rarely in our database.

[45] The inferred Lévy indices tend to scatter more when the cloud cover loosens up, e.g., on 11 May 2003. The scatter may thus indicate that the limiting case $\alpha = 1$ (dominated by direct transmission) occurs more frequently. Although anomalous diffusion yields the right limiting behavior ($\langle L_c \rangle \sim \Delta H$) as $\alpha \to 1$, we also observe many low values of τ_c^*. We should be cautious about applying any diffusion theory when $\tau_c^* \lesssim 1$.

[46] The cloud cover studied on 22 May 2003 demonstrates that the Lévy index α increases with increasing compactness and continuity of the cloud cover, viz. the stratus decks located between 350 and 3300 m ASL (Figure 13, with Figure 11). In this respect, it is evident that the optically much thinner cirrus deck (9000–10,000 m) on 22 May 2003 did not increase much the photon paths but in first instance acted as diffuser for the solar radiation [*Pfeilsticker et al.*, 1998b]. All these findings on photon path statistics are largely in agreement with earlier empirical findings by *Pfeilsticker* [1999] and *Min et al.* [2001], and it provides further evidence for the suggestion of *Davis and Marshak* [1997] on the nonclassical nature of photon path statistics under real cloud covers.

[47] Furthermore, the ratios we obtain for the RMS and mean photon paths $\sqrt{\langle L_c^2 \rangle}/\langle L_c \rangle$ (see Figures 8, 10, and 12) provide evidence that the numerical values of the exponents and prefactors in our hypothetical generalization of equations (16) and (18) is reasonably accurate for the predominant anomalous diffusion regime. Our findings thus largely confirm the two-moment calculus of the *Davis and Marshak* [2002] study, and it provides further evidence that the photon path statistics for real 3-D cloud covers requires elements of nonclassical (i.e., anomalous) diffusion transport physics.

[48] The data we used here was not selected to emphasize anomalous photon transport. Basically, it was just gathered from the time periods when all collocated instruments of interest were performing well. It is also important to note that, apart from the new focus on the second-order statistics of the path pdf, we have extended the parameter range of previous studies [*Pfeilsticker*,

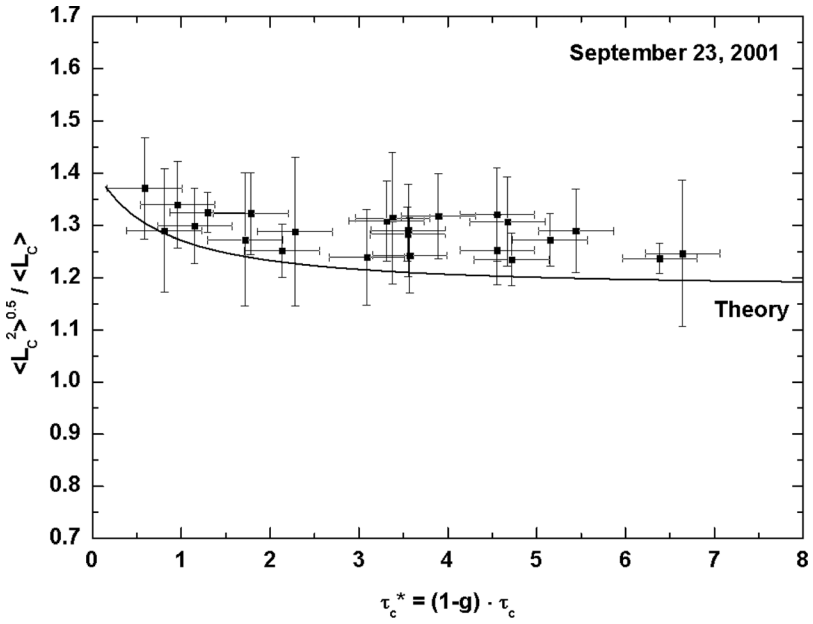

Figure 8. Ratio of inferred first two photon path length moments, $\langle L_c \rangle$ and $\sqrt{\langle L_c^2 \rangle}$, for the 23 September 2001 observations and comparison with the predicted ratio (line) based on the classical diffusion theory.

1999; *Min et al.*, 2001] to smaller mean optical depths, hence our interest in the preasymptotic correction terms and the prefactors.

6. Conclusions

[49] Employing high-resolution oxygen A band spectrometry, we investigate the first two statistical moments of the path length distributions of solar photons transmitted through cloudy skies to the ground. Our study confirms the suggestion of the *Davis and Marshak* [1997] theoretical study and of earlier observational path length studies by *Pfeilsticker* [1999] and *Min et al.* [2001] that, in general, under cloudy skies the first moment of the photon path length distribution scales as $\langle L_c \rangle \sim \Delta H \cdot (\tau_c^*)^{\alpha-1}$ with α ranging between 1 and 2. This phenomenology indicates

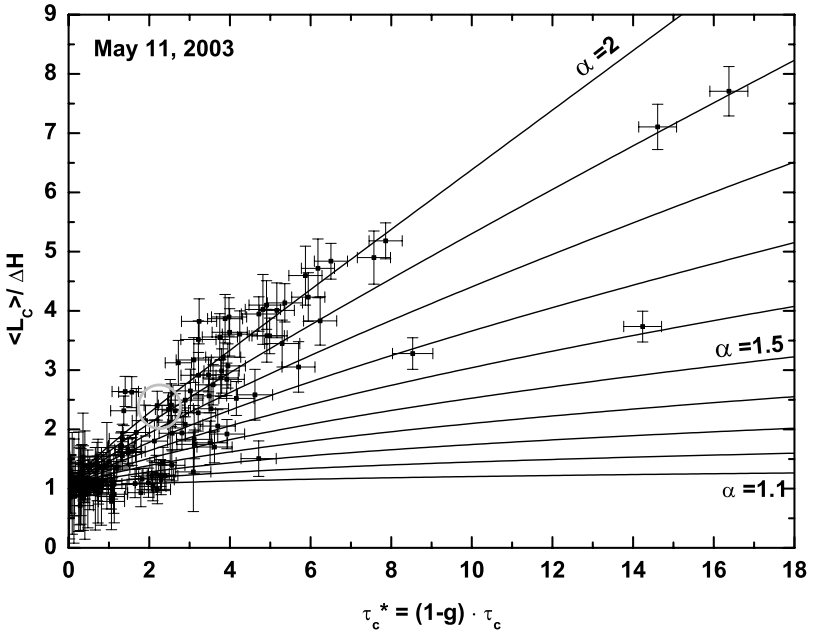

Figure 9. Mean cloud photon paths $\langle L_c \rangle$ as a function of effective cloud optical depth τ_c^* for the 11 May 2003 observation. The lines are prediction based on equation (16) modified as explained in the text for different values of the Lévy exponent $\alpha \leq 2$. The encircled point corresponds to the observation on 11 May 2003 at 1459 UT discussed in detail in the text.

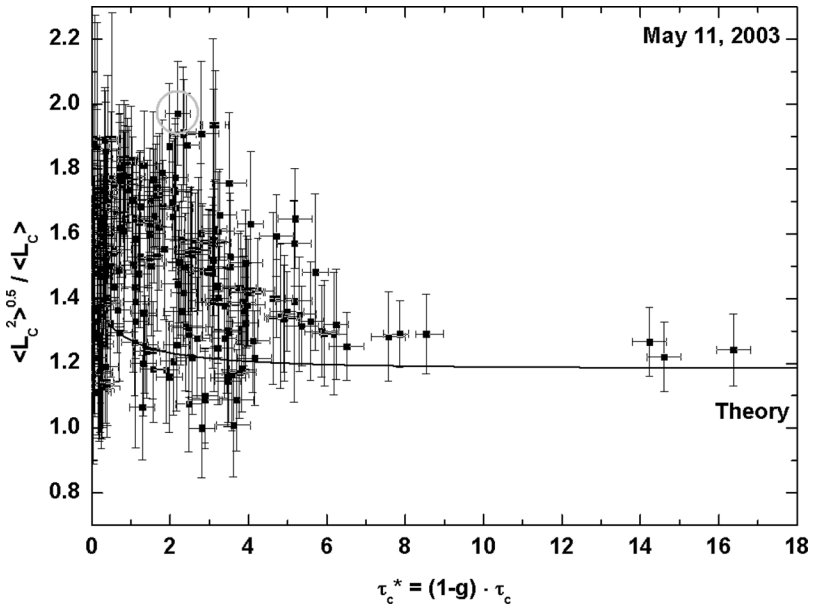

Figure 10. Ratio of inferred first two photon path length moments, $\langle L_c \rangle$ and $\sqrt{\langle L_c^2 \rangle}$, for the 11 May 2003 observations and comparison with the predicted ratio (line) based on the classical diffusion theory.

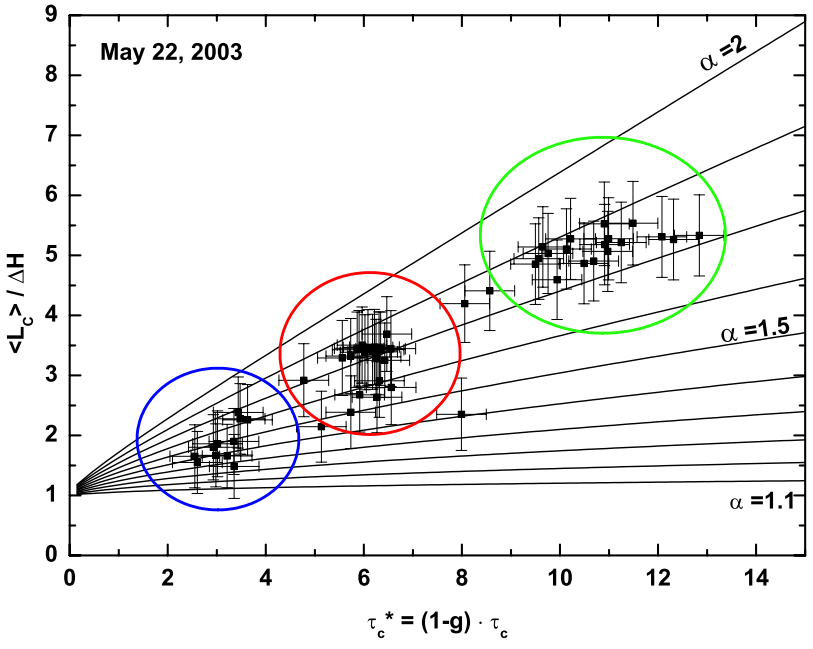

Figure 11. Mean cloud photon paths $\langle L_c \rangle$ as a function of effective cloud optical depth τ_c^* for the 22 May 2003 observation. The lines are prediction based on equation (16) modified as explained in the text for different values of the Lévy exponent $\alpha \leq 2$. The three data clusters (color coded blue, red, and green) correspond to the three different cloud situations probed between 1200 and 1223, 1223 and 1246, and 1246 and 1300 UT in Figure 10.

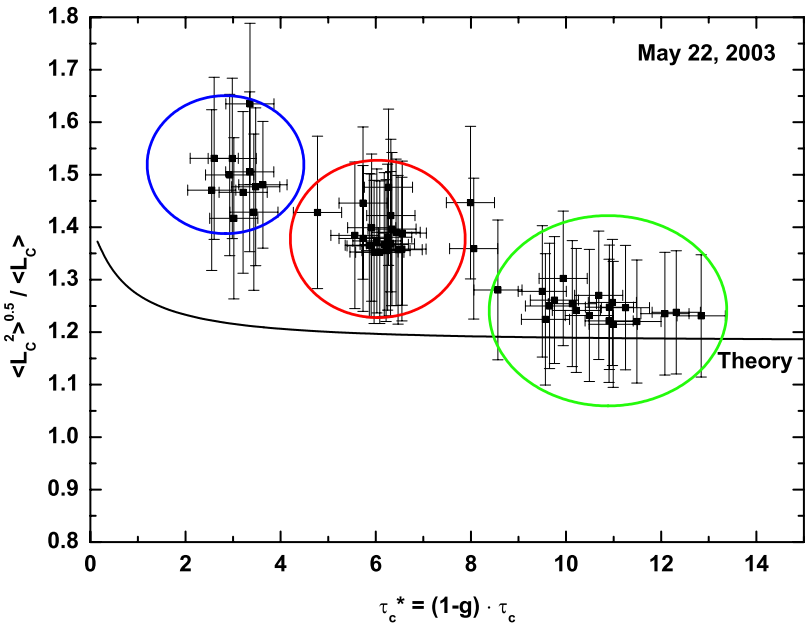

Figure 12. Ratio of inferred first two photon path length moments, $\langle L_c \rangle$ and $\sqrt{\langle L_c^2 \rangle}$, for the 22 May 2003 observations and comparison with the predicted ratio (line) based on the classical diffusion theory. The three data clusters (color coded blue, red, and green) are as in the Figures 11 and 12.

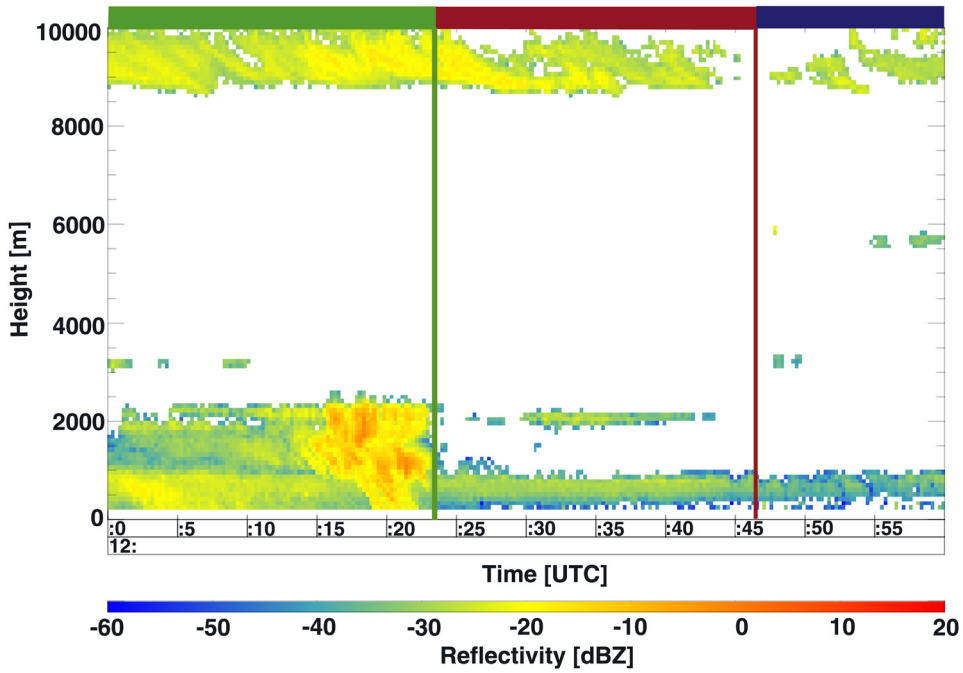

Figure 13. Zoom of measured radar reflectivities from from the KNMI 35 GHz radar for the 22 May 2003 observation in Figure 6.

that optically thick single cloud decks tend to show Lévy indices α compatible with 2, indicating classical photon transport. For more complex cloud covers that are multilayered and/or broken however, the transport is better characterized as anomalous, with the Lévy index α spanning values between 1 and 2. We also find that $\langle L_c^2 \rangle$ is only slightly greater than $\langle L_c \rangle^2$, irrespective of the cloud optical depth and of α. Thus our study confirms [*Davis and Marshak*, 2002] predictions for the values of the prefactors in the path length to optical depth relations for classical diffusion, and it suggests that they are not very different for the anomalous diffusion regime.

[50] Our study thus provides further evidence that cloudy-sky photon path lengths, and hence atmospheric absorption, require consideration of nonclassical photon transport theory. We anticipate applications in climate science and in other areas, such as atmospheric photochemistry, interested in amounts of absorption by well-mixed gases.

[51] **Acknowledgments.** We are grateful for the hospitality provided by the KNMI facility at Cabauw (NL) for the field campaign. In particular, we thank A. van Lammeren, A. Feijt, and J.-L. Brenguier for organizing both campaigns and for providing us with access to the Cabauw facility. Special thanks go to W. Hovius for perfectly running the field site. Financial support for the project came from the Bundesministerium für Bildung und Forschung through the AFO2000 project 4D-Wolken, grant 07 ATF24. A.D. acknowledges the U.S. DOE Atmospheric Radiation Measurement (ARM) program for sustained financial support. Finally, we have appreciated many fruitful discussions with A. Marshak, Q.-L. Min, L. Harrison, and P. Gabriel as well as the insightful comments by the anonymous reviewers.

References

Buldyrev, S. V., S. Havlin, A. Y. Kazakov, M. G. E. da Luz, E. P. Raposo, H. E. Stanley, and G. M. Viswanathan (2001), Average time spent by Lévy fights and walks on an interval with absorbing boundaries, *Phys. Rev. E*, *64*, 41,108.

Case, K. M., and P. F. Zweifel (1967), *Linear Transport Theory*, Addison-Wesley, Boston, Mass.

Crewell, S., H. Czekala, U. Löhnert, C. Simmer, T. Rose, R. Zimmermann, and R. Zimmermann (2001), Microwave radiometer for cloud carthography: A 22-channel ground-based microwave radiometer for atmospheric research, *Radio Sci.*, *36*, 621–638.

Crewell, S., et al. (2004), The Baltex Bridge Campaign—An integrated approach for a better understanding of clouds, *Bull. Am. Meteorol. Soc.*, *85*, 1565–1584.

Davis, A. B., R. F. Cahalan, A. Marshak, and W. J. Wiscombe (1997), The Landsat scale-break in stratocumulus as a three-dimensional radiative transfer effect, implications for cloud remote sensing, *J. Atmos. Sci.*, *54*, 241–260.

Davis, A. B., and A. Marshak (1997), Lévy kinetics in slab geometry: Scaling of transmission probability, in *Fractal Frontiers*, edited by M. M. Novak and T. G. Dewey, pp. 63–72, World Sci., Hackensack, N. J.

Davis, A. B., and A. Marshak (2001), Multiple scattering in clouds: Insights from three-dimensional diffusion/p_1 theory, *Nucl. Sci. Eng.*, *137*, 251–280.

Davis, A. B., R. F. Cahalan, J. D. Spinhirne, M. J. McGill, and S. P. Love (1999), Off-beam lidar: An emerging technique in cloud remote sensing based on radiative Green-function theory in the diffusion domain, *Phys. Chem. Earth B*, *24*, 241–260. (Erratum, *Phys. Chem. Earth B*, *24*, 757–765, 1999.)

Davis, A. B., and A. Marshak (2002), Space-time characteristics of light transmitted by dense clouds: A green function analysis, *J. Atmos. Sci.*, *59*, 2713–2727.

Donovan, D. P., A. C. A. P. van Lammeren, R. J. Hogan, H. W. J. Russchenberg, A. Apituley, P. Francis, J. Testud, J. Pelon, M. Quante, and J. Goddard (2001), Cloud effective particle size and water content profile retrievals using combined lidar and radar observations: 2. Comparison with IR radiometer and in situ measurements of ice clouds, *J. Geophys. Res.*, *106*, 27,449–27,464.

Fischer, J., and H. Grassl (1991), Detection of cloud-top height from backscattered radiances within the oxygen A band. Part 1: Theoretical study, *J. Appl. Meteorol.*, *30*, 1245–1259.

Fischer, J., W. Cordes, A. Schmitz-Peiffer, W. Renger, and P. Morel (1991), Detection of cloud-top height from backscattered radiances within the oxygen A band. Part 2: Measurements, *J. Appl. Meteorol.*, *30*, 1260–1267.

Funk, O. (2000), Photon pathlengths distributions for cloudy skies pxygen: A-band measurements and radiative transfer model calculations, Ph.D. thesis, Univ. of Heidelberg, Heidelberg, Germany.

Funk, O., and K. Pfeilsticker (2003), Photon path length distributions for cloudy skies: Oxygen A-band measurements and model calculations, *Ann. Geophys.*, *21*, 615–626.

Grechko, Y. I., V. I. Dianov-Klokov, and I. P. Malkov (1973), Aircraft measurements of photon paths in reflection and transmission of light by clouds in the 0.76 μm oxygen band, *Atmos. Ocean Phys.*, *9*, 262–265.

Harrison, L. C., and Q.-L. Min (1997), Photon pathlengths from O_2 A-band absorption, in *IRS'96: Current Problems in Atmospheric Radiation*, pp. 594–598, A. Deepak, Hampton, Va.

Heidinger, A. K., and G. L. Stephens (2000), Molecular line absorption in a scattering atmosphere. Part II: Application to remote sensing in the O_2 A-band, *J. Atmos. Sci.*, *57*, 1615–1634.

Heidinger, A. K., and G. L. Stephens (2002), Molecular line absorption in a scattering atmosphere. Part III: Path length characteristics and the effects of spatially heterogeneous clouds, *J. Atmos. Sci.*, *59*, 1641–1654.

Kurucz, R. L., I. Furenlid, J. Brault, and L. Testerman (1984), *Solar Flux Atlas From 296 to 1300 nm*, Natl. Sol. Obs., Sunspot, N. M.

Lovejoy, S., and B. B. Mandelbrot (1985), Fractal properties of rain and a fractal model, *Tellus, Ser. A*, *37*, 209–232.

Marshak, A., A. Davis, R. F. Wiscombe, and W. J. Cahalan (1995), Radiative smoothing in fractal clouds, *J. Geophys. Res.*, *100*, 26,247–26,261.

Min, Q.-L., and L. C. Harrison (1999), Joint statistics of photon path length and cloud optical depth, *Geophys. Res. Lett.*, *26*, 1425–1428.

Min, Q.-L., L. C. Harrison, and E. Clothiaux (2001), Joint statistics of photon pathlength and cloud optical depth: Case studies, *J. Geophys. Res.*, *106*, 7375–7386.

Min, Q.-L., and E. Clothiaux (2003), Photon path length distributions inferred from rotating shadowband spectrometer measurements at the atmospheric radiation measurements program southern great plains site, *J. Geophys. Res.*, *108*(D15), 4465, doi:10.1029/2002JD002963.

Min, Q.-L., L. C. Harrison, P. Kiedron, J. Berndt, and E. Joseph (2004), A high-resolution oxygen A-band and water vapor spectrometer, *J. Geophys. Res.*, *109*, D02202, doi:10.1029/2003JD003540.

O'Brien, D. M., and R. M. Mitchell (1992), Error estimates for retrieval of cloud top pressure using absorption in the A-band of oxygen, *J. Appl. Meteorol.*, *31*, 1179–1192.

Pfeilsticker, K. (1999), First geometrical path lengths probability density function derivation of the skylight from spectroscopically highly resolving oxygen Aband observations: 2. Derivation of the Lévyindex for the skylight transmitted by midlatitude clouds, *J. Geophys. Res.*, *104*, 4101–4116.

Pfeilsticker, K., F. Erle, O. Funk, L. Marquard, T. Wagner, and U. Platt (1998), Optical path modifications due to tropospheric clouds: Implications for zenith sky measurements of stratospheric gases, *J. Geophys. Res.*, *103*, 25,323–25,335.

Pfeilsticker, K., F. Erle, O. Funk, H. Veitel, and U. Platt (1998), First geometrical path lengths probability density function derivation of the skylight from spectroscopically highly resolving oxygen aband observations: 1. Measurement technique, atmospheric observations, and model calculations, *J. Geophys. Res.*, *103*, 11,483–11,504.

Platt, U. (1994), Differential optical absorption spectroscopy (DOAS), in *Air Monitoring by Spectroscopic Techniques*, *Chemical Anal. Ser.*, vol. 127, edited by W. M. Sigrist, pp. 27–84, John Wiley, Hoboken, N. J.

Platt, U., and J. Stutz (2004), *Differential Optical Absorption Spectroscopy (DOAS): Principle and Applications*, Springer, New York.

Polonski, I. N., and A. B. Davis (2004), Lateral photon transport in dense scattering and weakly-absorbing media of finite thickness: Asymptotic analysis of the space-time Green function, *J. Opt. Soc. Am. A Opt. Image Sci.*, *21*, 1018–1025.

Portmann, R. W., S. Solomon, R. W. Sanders, J. S. Daniel, and E. G. Dutton (2001), Cloud modulation of zenith sky oxygen path lengths over Boulder, Colorado: Measurements versus model, *J. Geophys. Res.*, *106*, 1139–1155.

Quante, M., H. Lemke, H. Flentje, P. Francis, and J. Pelon (2000), Boundaries an internal structure of mixed phase clouds as deduced from ground-based 95-GHz radar and airborne lidar measurements, *Phys. Chem. Earth*, *25*(10–12), 889–895.

Rose, T., S. Crewell, U. Löhnert, and C. Simmer (2005), A network suitable microwave radiometer for operational monitoring of the cloudy atmosphere, *Atmos. Res.*, *7*, 183–200.

Rothman, L., et al. (2003), The HITRAN molecular spectroscopic database: Edition of 2000 including updates though 2001, *J. Quant. Spectrosc. Radiat. Transfer*, *82*, 5–44.

Samorodnitsky, G., and M. S. Taqqu (1994), *Stable Non-Gaussian Random Processes*, CRC Press, Boca Raton, Fla.

Schmidt, S., K. Lehmann, and M. Wendisch (2004), Minimizing instrumental broadening of the drop size distribution with the m-fast-fssp, *J. Atmos. Oceanic Technol.*, *21*, 1855–1867.

Shlesinger, M. F., G. M. Zaslavsky, and U. Frisch (1995), *Lévy Flights and Related Topics in Physics*, Springer, New York.

Stephens, G. L., and A. K. Heidinger (2000), Molecular line absorption in a scattering atmosphere. Part I: Theory, *J. Atmos. Sci.*, *57*, 1599–1614.

Stephens, G. L., A. K. Heidinger, and P. M. Gabriel (2005), Photon paths and cloud heterogeneity: An observational strategy to assess effects of 3D geometry on radiative transfer, in *3D Radiative Transfer in Cloudy Atmospheres*, edited by A. Marshak and A. B. Davis, pp. 587–627, Springer, New York.

Stutz, J., and U. Platt (1996), Numerical analysis and estimation of the statistical error of differential optical absorption spectroscopy measurements with least-squares methods, *Appl. Opt.*, *35*, 6041–6053.

Van de Hulst, H. C. (1980), *Multiple Light Scattering, Tables, Formulas and Applications, Vol. 2*, Elsevier, New York.

Veitel, H., O. Funk, C. Kurz, U. Platt, and K. Pfeilsticker (1998), Geometrical pathlength probability density functions of the skylight transmitted by midlatitude cloudy skies: Some case studies, *Geophys. Res. Lett.*, *25*(17), 3355–3358.

von Savigny, C., O. Funk, U. Platt, and K. Pfeilsticker (1999), Radiative smoothing in zenith-scattered skylight transmitted to the ground, *Geophys. Res. Lett.*, *26*, 2949–2952.

S. Crewell and U. Löhnert, Meteorological Institute, University of Munich, Theresienstrasse 37, D-80333 Munich, Germany.

A. B. Davis, Space and Remote Sensing Sciences Group, Los Alamos National Laboratory, Los Alamos, NM 87545, USA.

H. Klein Baltink, Royal Netherlands Meteorological Institute (KNMI), Postbus 201, 3730 AE De Bilt, Netherlands.

J. Meywerk and M. Quante, GKSS Research Centre, Max-Planck-Strasse, D-21502 Geesthacht, Germany.

K. Pfeilsticker and T. Scholl, Institut für Umweltphysik, INF 229, University of Heidelberg, D-69120 Heidelberg,Germany. (klaus.pfeilsticker@iup.uni-heidelberg.de; thomas.scholl@iup.uni-heidelberg.de)

C. Simmer, Meteorological Institute, University of Bonn, Auf dem Huegel 20, D-53121 Bonn, Germany.